Macro/Micro-pore structure characteristics and the chloride penetration of self-compacting concrete incorporating different types of filler and mineral admixture

Mahmoud Khashaa Mohammed*, AndrewRobert Dawson, Nicholas Howard Thom****

*corresponding author

School of Civil Engineering, Faculty of Engineering, University of Nottingham, University Park, Nottingham NG7 2RD UK, E-mail: evxmkm@nottingham.ac.uk, Lecturer, University of Anbar, Iraq, Faculty of Engineering, E-mail: mahmoudkh_ani@yahoo.com

**** Co-authors***

School of Civil Engineering, Faculty of Engineering, University of Nottingham, University Park, Nottingham NG7 2RD UK. Department

Abstract

The relationship between the internal pore structure features at different scales and the local micro-characteristics of the interfacial transition zone (ITZ) to the non-steady state chloride migration coefficient (D_{nssm}) is investigated for one normal and three types of sustainable high performance self-compacting concrete mixes. The pore structure classification at different scales and the percolation degrees of the ITZ's pores were determined using both vacuum-saturated and mercury intrusion porosimetry (MIP) techniques. Further, the local micro-permeation features of the ITZ, such as thickness, porosity and the chemistry of its hydration products is examined using the SEM coupled with the EDX analysis on polished, carbon-coated, flat specimens. Chloride movement was achieved using a modified rapid migration test.

It was deduced that the degree of percolation of the pores of the ITZ had a significant role in controlling the chloride penetration process. Further, it is proposed that the ITZ thickness

might be, primarily, responsible in determining the chloride ions' migration velocity especially when coarse and unreactive filler is used. At nano scale, it is also suggested that the critical pore diameter in the cement matrix is more significant than is the average pore diameter in controlling the chloride resistance in SCC.

Keywords: Chloride penetration, rapid migration test, self-compacting concrete; microstructure; interfacial transition zone; cement replacement, pores percolation

1. Introduction

As reported by many investigations, the chloride ion penetration from an external source (sea, underground and de-icing water) is considered as one of the main causes of the initiation of steel reinforcement corrosion which then leads to reduction in the serviceability life of the affected concrete structure. This topic has become an increasingly important area in the study of concrete durability since the middle of the last century[1]. With the widespread use of SCC, which is relatively a new type of concrete, in different concrete structures exposed to severe chloride environments such as bridges, culverts, tunnels, tanks, dams, and precast concrete products, much information is needed to assess the chloride ingress and its relationship to the concrete's internal microstructure at macro, micro and even at Nano-scales.

Since concrete/mortar is considered as a porous composite material with three different phases (cement matrix, aggregate and ITZ between them), the chloride ions can penetrate the concrete through the continuous pores of each phase. The aggregate phase (fine/coarse) has less effect on the chloride penetration due to the lower diffusion coefficient in comparison with cement matrix [2]. However, from a mix design point of view, the existence of high amounts of aggregate (high volume fraction) could have two, conflicting, effects on the transport properties of the concrete including the chloride movement. On the one hand, it leads to more numerous ITZs, and more volume of this region, which may assist the chloride

ion movement due to the high porosity in compression with the background matrix porosity. On the other hand, it increases the tortuosity of penetration paths through the matrix [3]. It is known that the SCC has a dense microstructure due to the use of low water to cementatious material ratios, and a dense cement matrix containing reactive and non-reactive fillers as compared with normal vibrated concrete (NVC) [4, 5]. Although SCC sometimes had the same or higher water to cementatious material ratio as a NVC, the use of fillers and mineral admixtures and high dosages of SP might also make the difference. Thus, the SCC could have a less easily penetrated microstructure. However, as reported by Assié et al. [6], referencing Zhu et al.[7], the modification of the microstructure might not be enough to assure sufficient resistance to the chloride penetration as this property might be governed by the tortuosity, the percolation and the connectivity of the internal pore network.

Although research work has been done to estimate the chloride penetration resistivity as part of the durability assessment of SCC, the available experimental data about the SCC showed that no definite conclusion could be drawn about whether SCC has similar, larger or smaller resistance to chloride penetration than NVC at the same strength level. Assié et al.[6] claimed that a SCC having a similar or, even better, compressive strength than a NVC, although at a higher w/c ratio, had equivalent chloride diffusion and water absorption. In their study, the SCC investigated employed limestone filler for all mixes. On the other hand, the results of Audenaert et al.[8] revealed that no definite conclusion was possible about whether SCC has a larger or smaller chloride migration coefficient in comparison with NVC. Recently, Dinakar et al.[9] noticed that, in spite of higher permeable voids and higher water absorption, high fly ash SCC showed lower chloride penetrability in comparison with NVC at any strength grade. The authors suggested that it could be as a result of a higher chloride binding capacity of the cement matrix caused by the presence of high available C_3A in the cementious materials system with increased fly ash content. .

Understanding the relationship between the microstructure of the concrete as it relates to degradation, especially chloride penetration and carbonation, still presents a great challenge for the concrete technologist. This is due to both the complexity of the chemistry and the microstructure of SCC, in particular the different macro/micro/nano scale characteristics and the complexities of these two physico-chemical phenomenon as well. For SCC, questions have been raised as to which has the dominant role: the micro permeation characteristics of the ITZ or the pore characteristics of the bulk cement matrix?

To attempt an answer to this question, Leemann et al. [10] studied the effect of using different types of cement on the porosity of the ITZ and its relationship to chloride resistance, using the rapid chloride migration test according to the Swiss standard SIA 262/1. In this study, the authors concluded that the change of the internal pore structure of the cement matrix, as caused by the use of different types of cement in SCC mixes, had a stronger effect on the non-steady state chloride migration coefficients obtained than did the pore volume in the ITZ. However, the long curing time (62 days) used in this investigation might reduce any controlling effect of the local microstructure characteristics of the ITZs. Moreover, Leemann et al. made no attempt to address how the change of the internal pore structure, including the tortuosity effect of the aggregate and the percolation of pores in the ITZ, nor the nature of the pore system in the matrices, could affect the chloride resistance of SCC as only one technique was used (Image analysis) for characterising the ITZ pores microstructure. This cannot give enough information about the effect of the internal capillary pores and their percolation to fully defend their conclusion. While the Leemann et al. results were based on the use of different cement types to examine the chloride resistivity of SCC, the current research work is designed to examine the effects of the internal microstructure and its role in determining the chloride ingress process in normal and sustainable high performance SCC.

In previous research work [11, 12] the authors have attempted to develop a further understanding of the relationship between carbonation and the microstructural properties of

sustainable SCC via accelerated tests. In the present paper they aim to quantitatively analyse the correlation between these characteristics, in terms of the internal pore structure and the local micro-permeation of the ITZ properties as consequence of a change of filler and mineral admixture type at high cement replacement percentages, to the chloride penetration velocity. To achieve this, a non-steady state accelerated test was modified from the recommendations of NT Build 492 - Nordtest method [13] and used in the present study. The modification, as described in Section 3.3, was mainly performed in order to reduce the time of the test to, as much as possible, avoid the change of the ionic composition of the pore water solution (pH value) due to the migration of the OH^- ions and hence, limiting the local chloride binding ability due to the difference in reactivity levels of the fillers and the mineral admixtures used through the relatively long time of the standard test. The main issues addressed in this paper are:

i) Effect of using different types of filler and mineral admixtures, at relatively high rates of cement replacement, on the internal pore structure and the local micro-permeation characteristics of ITZ of different types of SCC.

ii) Determination of the non-steady state chloride migration coefficient (D_{nssm}) for SCCs with different binder types using a modified rapid migration test.

iii) Macro/micro and nano internal pore structure property relationships with the D_{nssm}.

These issues have been studied in order to provide further understanding of the microstructure of the sustainable SCC and the part it plays in determining the resistance to chloride penetration.

2. Experimental

program 2.1 Materials

Ordinary Portland cement CEM I, 52.5 R conforming to EN 197-1 was used to produce all the SCC and mortars. Natural limestone filler (LP) from Longcliffe quarry (Derbyshire, UK), fly ash (FA) class F confirming to BS EN 450-1 produced by the Cemex Company and Densified

silica fume (SF) produced by the Elkem Microsilica Company were used as a fillers and mineral admixtures. Table 1 shows the chemical and physical properties of these materials. The mineralogical and microstructural properties of the cement, fillers and mineral admixtures were characterized using the XRD and SEM techniques respectively. Fig.1 a, b and c show selected SEM micrographs of both the cement and the SF at high magnification whilst Fig 2a and b show the XRD patterns obtained from these powders. For LP and FA, such SEM micrographs and XRD spectra are presented in an earlier paper [11]. The SEM micrographs revealed that the surface texture of both the cement and LP particles are extremely rugous, the particles also being angular in shape. In contrast, the FA particles are spherically shaped with a very smooth surface texture. The SF showed two particle shapes, first: spheroid agglomerates with diameter in the range between (5-25) μm, second: very fine particle agglomerations with diameters in the range between approximately (0.05-10) μm. These measurements were based on different micrographs at various magnifications. Both types of SF particles demonstrated a very rugous surface texture.

Using the XRD technique, the major compounds of the cement powder were identified from the XRD pattern: C_3S, C_2S in the form of calcium silicate, C_3A in the form of calcium aluminum oxide, C_4AF in the form of the Brownmillerite phase as well as Anhydrate ($CaSO_4$) from the gypsum which is usually added to the cement to control the setting process. The XRD traces clearly indicated that the LP consisted of purely (100 %) calcite phase without a presence of any amorphous material. On the other hand, the FA comprised a vitreous medium with two main crystalline phases: Quartz (SiO_2) and Mullite ($A_{l6}Si_2O_{13}$) with a presence of amorphous material. The distinct hump in the XRD pattern revealed the presence of amorphous silica [11]. The SF XRD pattern was completely different from those of LP and FA with very small peaks of Potassium Magnesium Silicate ($K_2MgSi_3O_8$) being detected. The absence of the peaks in the XRD-spectra of the SF signifies a very high proportion of amorphous silicon dioxide (SiO_2).

Local river quartz sand with a maximum particle size of 5 mm was used as a fine aggregate for both SCC and mortars. The specific gravity and the water absorption of this type of sand were 2.65 and 1.5 % respectively. Natural quartz uncrushed gravel with a nominal maximum size of 10 mm was used as coarse aggregate. The specific gravity and the water absorption of the gravel were 2.65 and 0.8 % respectively. Superplastcizer (SP) based on polycarboxylic ether (PCE) polymer, was used to maintain the required fresh properties of SCC.

2.2 Mix design and production of SCC

The mix design of SCC mixes and their fresh requirements are shown in Table2. All the mixtures were designed to have a compressive strength grade of 50–60 MPa. The main difference between the mixes was the type of the binder (cement for the reference-SCC and cement plus fillers or mineral admixtures at relatively high cement replacement for the other three mixes). Approximately 33% of cement was replaced for these mixes, the exact proportion of admixture and of the coarse aggregate content depending on the differences between the specific weights of binder materials. The SCC mortars contained the same constituent but without coarse aggregate. The water quantity for the mortar was reduced by about 0.8% (coarse aggregate absorption) in order to ensure the same available water content for the full concrete. The adopted SP dosages to maintain the required fresh properties were based on several trial mixes. After mixing and optimizing the fresh requirements in terms of slump flow, T_{50}, Bj and SI% for the concrete (See Table 2) and the mini slump flow for the mortars (240-300 mm), the fresh SCC and mortars were filled into the moulds in one go without any applied compaction, demoulded after 48 hours, and finally cured at 20±2 ºC in a water tank until the date of the test (28 days). For the compressive strength test, 100 mm cubes were used. The test was conducting according to BS EN 12390-3 [14] and the listed values represent an average of three readings.

3. Methodology and tests performed

3.1 Pore structure investigation

3.1.1 MIP test

Small pieces of mortar weighing (1- 3) g obtained from the middle part of 70 mm mortar specimens (near the core block that was used for preparing the flat polished sections as described in section 3-2) were used for Mercury Intrusion Porosimetry (MIP) testing. In order to stop the hydration, the specimens were dried at 100 ˚C for approximately 24 hours (until a constant weight was achieved as determined by a high sensitive balance) and then they were kept in sealed containers until the day of the test. A Micrometrics Autopore IV mercury porosimeter, which can detect the pores as small as 7 nanometers with a maximum pressure of 414 MPa, was used. The pressure step was applied for 10 seconds and the test was conducted on an average of 3 samples for each mix.

3.1.2 Vacuumed Saturated Porosity (Macro Porosity)

Mortar discs with dimensions of 60mm in diameter and 10-13 mm in depth, cut from original cylinders 120 mm tall was used to assess the Macro porosity. The mortar disks were vacuumed using 100 mb for 3 hours followed by 2 hours vacuumed with saturated $Ca(OH)_2$ solution and left until the second day. This was done to ensure a full saturation of all the pores in the tested specimens. The porosity % is calculated using Eq.1 [15].

$P = (B-A)/(B-C) \times 100$……. Eq. 1

P: Porosity, B: Saturated surface dry weight, A= Oven-dry weight, C= Saturated submerged weight

Completing the MIP results, the vacuum saturation results were used to deduce a complete picture about all the pore size ranges, as the larger pores that cannot be detected by the MIP test is considered as additional macro-pores. Thus, the percentage of macro/micro pores of the mixes was re-calculated (see Table 3).

3. 2 Microstructure of the ITZ

The ITZ microstructural examinations were conducted on a core block (20x20x15mm) obtained from the middle part of 70 mm mortar cubes. Full details can be found in an earlier paper [11]. The preparation steps of flat-polished epoxy-impregnated specimens as described by Kjellsen et al. [16] was followed carefully. The specimens were coated with carbon and then stored in a vacuum chamber until capturing the BSE images. A Philips XL 30 SEM fitted with an Oxford Instruments INCA model spectrometer for energy-dispersive X-ray (EDX) analysis was used with an accelerating voltage of 15–25 kV. Eight images were selected randomly at different aggregates' locations (at a magnification of 500X) and analysed for each mix in order to detect the ITZ porosity and thickness. The same image analysis procedure for duplicated BSE micrograph images as described more fully in an earlier paper was adopted[11]. However, the average upper porosity threshold values for all the analysed images were 80, 70, 50 and 60 for cement LP, FA and FA + SF matrix systems respectively. The defined upper threshold value was based on the recommendation of the overflow method as shown in Fig3. In a very recent work [17], this method is considered as an accurate method for the pore segmentation of the cement matrix with different types of blended cement. A T-distribution statistical analysis with a confidence interval of 95% was used to examine the results' accuracy as the images were randomly selected and the error bars in Fig.8 tends to confirm the regularity of the deduced porosity in the analyzed bands (each 10 µm from the aggregate interface).

For the chemical analysis of the ITZ, X-ray line spectrum analysis using EDX (energy dispersive X ray analysis system) linked with SEM as described by Erdem et al. [18] was performed to identify the main hydrous compounds in both the ITZ and cement matrix(CM). However, due to the inhomogeneous nature of the ITZ, 3 to 4 lines per different aggregate interface for each mix were analysed. The average detected Ca/Si values come from 30 to 40 values in different spots in the ITZ and the cement matrix regions. The upper and lower limits

obtained from the standard deviation about the mean values were adopted to determine the accuracy of the results (See Table 4).

The analyses were conducted each 5 μm along a line that crossed the aggregate, ITZ and the bulk matrix. Four EDX spectra were collected in the aggregate and 10 in the ITZ and cement matrix (See Fig. 4). Firstly, the BSE image was rotated using the control software of the Scanning Electron Microscope so the X-ray line spectrum was selected to be perpendicular to the ITZ. Secondly, an image was captured for the area of interest using the ENCA-EDX software. Then, the spectrum line was drawn and the acquisition time for the detection of all elements of each spectrum was set to 60 seconds. This allowed detection at each spectrum point on the three or four lines in approximately 60 to 75 minutes. Finally, ENCA- EDX software was used to assess the proportion of each of the following elements: Ca, Si, Al, S, Fe, Na, Mg, K and O. However, the oxygen was normalized by the software stoichiometry. These elements were used for the purpose of identifying the main cementitious compounds in the ITZs and the cement matrix (Fig 4 gives an example of one X-ray line analysed for the regular SCC). As reported by several investigators e.g. [18, 19], the C-S-H, CH and AFm products could be identified from knowing the Ca/Si ratio. The ranges of this ratio for the different products are: $0.8 \leq Ca/Si \leq 2.5$, $Ca/Si \geq 10$ and $Ca/Si \geq 4.0$ respectively.

3.3 Rapid chloride migration test

The same type of specimen that was used for the Marco porosity test in section 3.1.2 was used to determine the none-steady state chloride migration coefficient (D_{nssm}). Before the test, the mortar discs were vacuumed and saturated with a $Ca(OH)_2$ solution. The same arrangement as suggested by the Nordtest standard [13] as shown in Fig.5, was adopted in performing the experiment. However, the main difference is the dimension of the specimens, especially the thickness, which can affect the chloride penetration depth considerably. According to the

standard, the time of the test should be determined dependent on the initial reading of the current under an applied voltage of 30V.

First, a preliminary work was conducted on one sample of each mix with an external voltage of 30V to find the initial current (I_{30v}) and, hence, a suitable time for the modified test so that chloride does not breakthrough nor achieve only a shallow penetration depth through the sample. None of these samples produced an initial current in the range suggested by the standard due to the difference in thickness of the used specimens leading to different electrical resistance. The initial currents were all in the range 80-320 mA. Thus, the challenge was to find an appropriate time that would keep the chloride penetration within the thickness of the specimen (10-13) mm under the initial current. As stated by McGrath and Hooton[20], the calculated non-steady chloride penetration coefficient was reasonably constant over the voltage range tested up to 30 V. For the modified arrangement just described, 30 V would cause a considerably greater voltage gradient and this gave cause for concern regarding possible heat generation and consequential specimen damage which would affect chloride ingress. For this reason during the preliminary work, the temperature of the anolyte (0.3M NaOH) and the catholyte (10% NaCl) solutions was measured continuously using a thermocouple. The range of the recorded temperatures was 18.6 - 25.4 °C showing that there was no substantial change in the temperature of the specimen during the test. The standard [13] stipulates an operating temperature range of 20 to 25 °C, thus the modified arrangements appear acceptable in this respect.

Several trials were performed on each specimen for 6, 5, 4, 3, 2 or 1 hours. Finally, the test duration then was specified to be 1 h as the chloride penetration was within the thickness of specimen for all types of SCC mortars whereas complete breakthrough of the chloride occurred under larger test durations.

Fig.6 shows examples of some samples broken in half to expose an internal cross section and the use of 0.1 M silver nitrate solution indicator ($AgNO_3$). White silver chloride precipitation

(AgCl) on the split surface appeared clearly after 5-10 minutes where the chloride ions have penetrated. Then, the D_{nssm} was calculated as an average value of duplicated successful samples for each mix using the modified Nernst-Planck equation [13]:

$$D_{nssm} = \frac{0.0239(273+T)L}{(U-2)t}\left(x_d - 0.0238\sqrt{\frac{(273+T)L\,x_d}{U-2}}\right) \quad \text{..... Eq.2}$$

D_{nssm}: non-steady-state migration coefficient, $\times 10^{-12}$ m^2/s

U: absolute value of the applied voltage, V

T: average value of the initial and final temperatures in the anolyte solution, °C

L: thickness of the specimen, mm

x_d: average depth of penetration over central zone as revealed by AgCl coloring (see Fig 2) , mm

t: test duration, h

4. Results and discussions

4-1 Macro, Micro and Nano characteristics of the pore structure

The Mercury cumulative intrusion curves and their derivatives as shown in Fig 7 a, b and the normal vacuum porosities results were used to quantify the pore structure characteristics at different scales and are summarized Table3.

The MIP porosity natures of the SCC mixes were determined in which the micro pores is bigger than 65 %. At this percentage the refinement of the pore structure is expected as stated by Erdem et al. [21]. Further, all the detected critical pore diameters (CPDs) and the average pore diameters (APDs) were in the Nano scale.

The macro and micro pores percentages were firstly calculated from these cumulative intrusion versus pore diameter curves considering 0.1µm to be the boundary between these

pore classes and then they were corrected using the macro porosity results (normal vacuum method as described earlier). The results demonstrate that the sustainable high performance SCC exhibited a micro-porous nature except in the case of the LP-SCC. This may be compared with the R-SCC which, marginally, is classified as macro-porous nature. On the other hand, all the detected CPDs which might demonstrate the nature of the pores' interconnectivity were determined to be of nano scale and they can be considered to be in the cement matrix far away from the ITZ regions. For the MIP test, it is already reported [22] that the mercury is expected to intrude into the large pores in the ITZ region if they are percolated. Consequently, the smaller pores (including the smallest ones (CPD)) will be allocated in the nearby cement matrix. Conversely, this is not the case for non-percolated ITZ [22]. The results of the present study showed that in spite of the macro porosity nature, the R-SCC exhibited similar or lower CPD as compared to the FA-SCC and LP-SCC respectively. However, the FA-SF-SCC demonstrated the lowest critical pore diameter signifying the lowest cement matrix' pore percolation.

For the SCC mortars, the volume fraction of the fine aggregate should be between 40-50% in order to reduce the segregation and obtain the stability for the mix as reported by published guidance and research findings [23-25]. Therefore, the probability of the ITZ having percolating pores is likely to be high even when ITZ thickness is small. For the adopted aggregate : mortar volume fraction (49.7-51.2%), the experimental results obtained for the minimum detected ITZ-thickness (15 micron for FA-SF-SCC) was analysed in conjunction with a numerical model adopted by Winslow et al. [26] for concrete mortars with different aggregate volume fractions. The analysis revealed that the degree of ITZ pores interconnectivity is more than 78%. These degrees were approximately greater than 90%, 88% and 95% for the R, FA, and LP-SCC respectively. Thus, the chloride penetration might largely be governed by ITZ pores percolations in such a way that the tortuosity effect of the

aggregate could be neglected due to the use of same volume fractions of all the mixes. The change in tortuosity effect of the aggregate is not entirely eliminated, but should be too small.

4.2 ITZ micro characteristics (Thickness, Porosity)

Fig. 8 shows the detected porosity profiles of the ITZs regions for the different SCCs as a function of the distance from the aggregate-cement paste interface up to 50 µm. These curves were used to determine both the approximate thickness and porosity of the ITZs. The exact determination of the ITZ thickness is difficult and not straightforward, with various proposed methods [10, 27, 28]. In the present study, the ITZs thicknesses were determined using the image analysis procedure described by Mohammed et al.[11]. In general, the analysis showed that all the deduced ITZs-thicknesses were less than 30 µm for the SCC mixes including that made with normal Portland cement (R-SCC). They were approximately 19.9 µm, 27.5 µm, 18.5 µm and µm 15 µm for R, LP, FA and FA-SF self-compacting concretes respectively. Olivier et al. [27]stated that the typical thickness of the ITZ region is about 50 µm for OPC paste in NVC so these SCC values are much smaller. At a microscopic scale, the absence of vibration, which is the case of SCC, could play an essential role in reducing the volume of the localized water around the aggregate surface[29]. This might explain the small thicknesses of the ITZ in all the investigated types of SCC. Nevertheless, relative to the R-SCC without cement replacement, the FA and FA-SF-SCC exhibited similar or slightly smaller ITZ thicknesses respectively. A higher amount of anhydrous cement was observed beyond the ITZ thickness of the R-SCC (Fig.6) indicating a higher local (ITZ) water to cement ratio which reduced the effective water content outside the ITZ leading to incomplete cement grain hydration. Thus, a higher ITZ thickness might be expected. It was already supposed by Laugesen (1993), quoted by Scrivener and Nemati [30], that the difference in the amount of anhydrous cement in the bulk cement matrix and the ITZ could be produced by the differences in the amount of water adhering to the aggregate surface.

However, the increase in ITZ thickness in the case of using LP as a partial replacement of cement, relative to the other three mixes, could suggest a "dilution" effect provided by the large LP unreactive grains in the ITZ. Also the presence of high amounts of CH or unreactive LP and the lack of CSH gels in this region was deduced for LP-SCC with the selected percentage of cement replacement, as explained in the previous paper [10].

ITZs porosities between 14.5-25 % were deduced for the investigated normal and sustainable high performance SCC within the detected ITZ thicknesses (Fig.8). Although the same water to binder ratio is adopted for all the mixes, the use of different types of fillers and mineral admixtures at high cement replacement has generated different ITZ porosities. This may attributed to both a physical filling effect and the chemical activity of the fillers and mineral admixtures used. R-SCC presented the highest ITZ porosity as compared with the other mixes and this might be related to the high ITZ local water as mentioned above.

Generally, the higher porosity of the ITZ might be related to the inability of the anhydrous cement grains to pack very well with the smooth surface of the aggregate due to the wall effect [27]. This concept might be different when reactive and non-reactive fillers are used leading to reduce the ITZ localised water. However, the inability of the hydration products to achieve a complete packing with the aggregate boundary might also be the cause of a porous interface. Therefore, the deduced ITZ-porosities using the image analysis were supported by the examination of the chemistry of the ITZ. The slight reduction in the ITZ porosity for the FA-SCC relative to R-SCC might indicate the inability of the FA to improve the ITZ chemistry. In contrast, FA-SF-SCC showed lower ITZ porosity relative to the FA-SCC and this suggests that the reduction of the ITZ porosity may be as a result of the filling effect of the very fine grains of SF improving the packing ability of the cement particles near the aggregate surface. The chemical analysis of the ITZs in the next section also showed a substantial modification in the chemistry of the ITZ especially in the FA-SF-SCC.

4.3 ITZ Chemistry

The chemical compositions of the ITZ and the cement matrix (CM) were investigated using the EDX-technique as described earlier. Table 4 summarizes the average Ca/Si ratios across the thickness of the ITZ and in the background cement matrix.

The analysis showed that the average Ca/Si ratio in the ITZ of the FA-SCC was greater than that which identifies the presence of CSH gel demonstrating a presence of considerable amount of CH. However, the ITZ of the FA-SCC showed a lower ITZ porosity than that of R-SCC and this may be due to the microstructural packing effect of the small spherical particles of FA. As reported by Zhang et al. [31], the packing state might be affected by the addition of pozzolans and decrease the amount of water that is needed for void filling and this might depend on the grain size of the pozzolanic material. This proposes that the improvement of the ITZ chemistry due to the high replacement of cement by FA may be attributed to the filling effect of the small particles of the FA only. However, it is known that the amorphous silica in the pozzolanic materials can consume the CH in the presence of water and produce another form of CSH gel or, at the least it can change the orientation of the large CH crystals. Consequently, further chemical development may occur. The chemical activity of the FA due to the amorphous silica detected by the XRD spectra recommends that full modification of the matrix in this region will take longer than 28 days, hindering a full comparison with the normal SCC in which hydration will be largely complete by that time.

The chemical analysis also indicated that incorporation of the combined partial replacement of cement by SF+FA led to the formation of an extraordinary quantity of CSH gel in the ITZ where the detected Ca/Si ratio was less than 2.08%. This may explain the lower detected ITZ thickness and lower porosity in this type relative to the other mixes. The EDX analysis also indicated a presence of high amount of CH or unreacted LP in the ITZ of the LP-SCC. The deduced average Ca/Si ration was greater than 14.43 indicating a dilution effect to this region which might cause an increase in ITZ thickness as explained in details in a previous work [11]

4.4 Relationships between the chloride penetration and the microstructure

In order to establish microstructure property relationships with the obtained chloride migration coefficients (D_{nssm}), an overview of the results obtained in the previous sections are summarised all together in Table 5.

Fig. 9 plots the relationships between ITZ porosity and thickness of the different SCC and the chloride migration coefficient. It can be seen clearly that the migration coefficient is simply related to ITZ thickness and, with the exception of the anomalous LP result discussed earlier, to the ITZ porosity. The latter relationship is in line with Jiang et al. [32] who stated that the increase of the porosity of the ITZ could facilitate the penetration of destructive agents including chloride and carbon dioxide. Taking the two relationships together, and assuming the distribution of the pores through the ITZ thickness around the aggregate, this might suggest that the chloride penetration in all types of SCC is likely to be controlled by the pore percolation in the ITZs, as a high degree of interconnected pores were deduced (78-95 %) in this region (Section 4.1). For LP-SCC, the higher ITZ thickness allows more capillary pores to be interconnected to adjacent ITZs in this mix type. Thus, a more porous path is anticipated and, thus, a decreased chloride resistance for this mix.

Fig.10 plots the relationships between the CPDs, the APDs and the chloride migration coefficients of the SCC. A broadly linear relationship was observed in both cases. Although the figure shows that the chloride migration coefficient had a higher correlation with the critical pore diameters than the average pore diameters, there are insufficient data to assess the relative reliability of these correlations. Moon et al. [33] observed a very high correlation (0.91) between the average pore diameter and the chloride diffusion coefficient for some high performance concrete specimens. On the basis of the present investigation alone, it would seem that the CPD in the cement matrix is a more important factor than the average pore diameter in controlling the chloride penetration velocity of SCC. Therefore, it is proposed that the chloride resistance of a SCC with high replacement of cement could be increased

/decreased according to the ability of its filler or mineral admixture to alter the interconnectivity nature of the pores in the cement matrix (CPD at the nano scale). This is independent on the resulting average capillary pores diameter in the ITZ and the cement matrix at this scale or the porosity value/nature and of the pore diameters at the micro or macro scales.

5. Conclusion

Based on the results obtained in this investigation, the following concluding remarks are derived:

- The use of LP at relatively high replacement of cement increased the chloride penetration velocity of LP-SCC as compared with both the use of cement only (without any replacement) and the incorporating of mineral admixture such as FA and FA+SF at the same replacement percentage.
- The ITZ micro characteristics for the investigated SCCs suggest that the use of a low water to binder ratio might be primarily responsible for determining the ITZ thickness while the agglomerations of the coarser unreacted LP near the aggregate-paste interface might also contribute to increasing the ITZ thickness. Further, the internal pore structure analysis at different scales and micro-permeation properties of the ITZ also indicated a diluting effect of this filler type in both the ITZ and the cement matrix as well.
- The average Ca/Si ratios in the ITZ regions (3.4, 3.6 and 14.43) for the R, FA and LP SCCs respectively revealed substantial amounts of CH. However, the reduced presence of this compound in the FA-SF-SCC suggests that the ITZ of this mix contains a high amount of CSH gel with an average Ca/Si of 2.08 only.
- The modification in the chemistry of the ITZ due to the use of different fillers and mineral admixture as a high partial replacement leads to different ITZ porosities. This was more noticeable in the case of using the FA+SF replacement rather than when using the simple FA or LP replacement.

- The chloride migration coefficient was proportional to both the thickness and the porosity of the ITZ. However, the ITZ porosity of the LP-SCC did not fit with this relation. This suggests that high deduced ITZ thickness increased the capillary pore's percolation in the ITZ and thus ITZ thickness was more responsible than ITZ porosity alone in determining the chloride ingress.
- The internal pore structure analysis at different scale revealed that the macro or micro porosity natures of the SCC did not relate to the chloride penetration resistivity as it is the interconnectivity of the pores in the cement matrix (represented by the change in the CPD) and the percolation degree of the pores in the ITZ that play a more important controlling role.
- At the nano-scale, the comparison of the results of the chloride migration assessment and of the characteristics of the internal pore structure demonstrated that the chloride penetration velocities were more closely related to the change in the CPDs in the cement matrix than to the APDs, including the capillary pores, in both the ITZ and the cement matrix as detected by the MIP.

Acknowledgements

The principal author would like to express his gratitude for his PhD scholarship sponsored by Higher Committee for Education Development in Iraq (HCED). The authors would like to gratefully acknowledge Mr Keith Dinsdale (Chief Experimental Officer, University of Nottingham - Faculty of Engineering), and Dr Nigel Neate (University of Nottingham - Faculty of Engineering) for their valuable help in conducting the MIP and SEM tests. Thanks should also go to Mr Jason Heaton a member of the Department of Electrical and Electronic Engineering, University of Nottingham for his help in the arrangement of the accelerated chloride penetration test. The authors also wish thank Mr Richard Blakemore (Senior Technician in NTEC, Faculty of Engineering) and Miss Nancy Milne and Mr Tom Buss (both Technicians, Faculty of Engineering) for their help in cutting and preparation of the concrete and SEM samples.

Captured figures and tables

Figure 1 Selected SEM micrographs of: a) Cement b) Silica fume C) silica fume at high magnification

Figure 2 XRD spectra for: a) Cement b) Silica fume

Figure 3 Example of the selection of upper porosity threshold using overflow method

Figure 4 Example of X-ray line spectrum analyses (one line analysis for R-SCC)

Figure 5 Photographs and schematic diagram for the rapid chloride migration test

Figure 6 Examples of some tested specimens and the chloride penetration distance (xd) revealed by AgCl

Figure 7 Mercury intrusion curves b) Derivatives of Mercury intrusion curves

Figure 8 ITZ porosity profiles for the mixes

Figure 9 Relationship between the chloride migration coefficients, ITZs thicknesses and ITZs porosities

Figure 10 Relationship between the chloride migration coefficients and pore structure characteristics

Tables

Table 1 Chemical and physical properties of the used cement, fillers and mineral admixtures Table 2 Mix design and fresh requirements of SCC mixes

Table 3 Internal pore characterizations at different scales (macro/micro and nano)

Table 4 Average Ca/Si ratio in the ITZ and cement matrix for SCC

Table 5 Overview of the pore structure, the ITZ features and the chloride migration coefficient results

References

1. Angst, U., B. Elsener, C.K. Larsen, and Ø. Vennesland, *Critical chloride content in reinforced concrete — A review.* Cement and Concrete Research, 2009. **39**(12): p. 1122-1138.
2. Shi, X., N. Xie, K. Fortune, and J. Gong, *Durability of steel reinforced concrete in chloride environments: An overview.* Construction and Building Materials, 2012. **30**(0): p. 125-138.
3. Delagrave, A., J. Bigas, J. Ollivier, J. Marchand, and M. Pigeon, *Influence of the interfacial zone on the chloride diffusivity of mortars.* Advanced Cement Based Materials, 1997. **5**(3): p. 86-92.
4. Coppola, L., T. Cerulli, and D. Salvioni, *Sustainable development and durability of self-compacting concretes.* Fly ash, silica fume, slag and natural pozzolans in concrete, 2004: p. 29-50.
5. Yazıcı, H., *The effect of silica fume and high-volume Class C fly ash on mechanical properties, chloride penetration and freeze–thaw resistance of self-compacting concrete.* Construction and Building Materials, 2008. **22**(4): p. 456-462.
6. Assie, S., G. Escadeillas, and V. Waller, *Estimates of self-compacting concrete 'potential'durability.* Construction and Building Materials, 2007. **21**(10): p. 1909-1917.
7. Zhu, W., J. Quinn, and P. Bartos. *Transport properties and durability of self-compacting concrete*. in *Proceedings of the second international symposium on self-compacting concrete*. 23–25 October 2001. Tokyo, Japan.
8. Audenaert, K., V. Boel, and G. De Schutter, *Chloride migration in self compacting concrete.* 2007.
9. Dinakar, P., K.G. Babu, and M. Santhanam, *Durability properties of high volume fly ash self compacting concretes.* Cement and Concrete Composites, 2008. **30**(10): p. 880-886.
10. Leemann, A., R. Loser, and B. Münch, *Influence of cement type on ITZ porosity and chloride resistance of self-compacting concrete.* Cement and Concrete Composites, 2010. **32**(2): p. 116-120.
11. Mohammed, M.K., A.R. Dawson, and N.H. Thom, *Production, microstructure and hydration of sustainable self-compacting concrete with different types of filler.* Construction and Building Materials, 2013. **49**(0): p. 84-92.

12. Mohammed, M.K., A.R. Dawson, and N.H. Thom, *Carbonation of filler typed self-compacting concrete and its impact on the microstructure by utilization of 100% CO2 accelerating techniques.* Construction and Building Materials, 2014. **50**(0): p. 508-516.
13. Nordtest.NT BUILD 492, *Concrete mortar and cement based repair materials:chloride migration coefficient from non-steady-state migration experiments*. 1999.
14. BS EN 12390-3, *Testing hardened concrete part3: Compressive strength of test specimens*. 2002, British Standard Institution.
15. Khan, M.I., *Novel method for measuring porosity of high strength concrete*, in *strength concrete. Proceedings of the 7th Saudi Engineering Conference (SEC7)*. 2004.
16. Kjellsen, K., A. Monsøy, K. Isachsen, and R. Detwiler, *Preparation of flat-polished specimens for SEM-backscattered electron imaging and X-ray microanalysis—importance of epoxy impregnation.* Cement and Concrete Research, 2003. **33**(4): p. 611-616.
17. Gao, Y., G. De Schutter, G. Ye, H. Huang, Z. Tan, and K. Wu, *Porosity characterization of ITZ in cementitious composites: concentric expansion and overflow criterion.* Construction and Building Materials, 2013. **38**: p. 1051-1057.
18. Erdem, S., A.R. Dawson, and N.H. Thom, *Impact load-induced micro-structural damage and micro-structure associated mechanical response of concrete made with different surface roughness and porosity aggregates.* Cement and Concrete Research, 2012. **42**(2): p. 291-305.
19. Rossignolo, J.A., *Interfacial interactions in concretes with silica fume and SBR latex.* Construction and Building Materials, 2009. **23**(2): p. 817-821.
20. McGrath, P. and R. Hooton, *Influence of voltage on chloride diffusion coefficients from chloride migration tests.* Cement and Concrete Research, 1996. **26**(8): p. 1239-1244.
21. Savas, E., *Impact Load-Induced Microstructural Damage of Concrete Made with Unconventional Aggregates*. 2012, University of Nottingham: UK.
22. Shane, J.D., T.O. Mason, H.M. Jennings, E.J. Garboczi, and D.P. Bentz, *Effect of the interfacial transition zone on the conductivity of Portland cement mortars.* Journal of the American Ceramic Society, 2000. **83**(5): p. 1137-1144.
23. EFNARC, S., *Guidelines for Self-Compacting Concrete.* European Federation for Specialist Construction Chemicals and Concrete Systems, Farnham, UK, 2002: p. 32.

24.Koehler, E.P. and D.W. Fowler. *ICAR Mixture Proportioning Procedure for Self-Consolidating Concrete*. 2006 04-05-2012]; Available from: http://www.icar.utexas.edu/publications/108/ICAR%20108-1%20(Proportioning).pdf.

25. De Schutter, G., P.J.M. Bartos, P. Domone, and J. Gibbs, *Self-compacting concrete*. 2008: Taylor and Francis Group.

26. Winslow, D.N., M.D. Cohen, D.P. Bentz, K.A. Snyder, and E.J. Garboczi, *Percolation and pore structure in mortars and concrete.* Cement and Concrete Research, 1994. **24**(1): p. 25-37.

27. Ollivier, J., J. Maso, and B. Bourdette, *Interfacial transition zone in concrete.* Advanced Cement Based Materials, 1995. **2**(1): p. 30-38.

28. Gao, Y., G. De Schutter, G. Ye, H. Huang, Z. Tan, and K. Wu, *Characterization of ITZ in ternary blended cementitious composites: Experiment and simulation.* Construction and Building Materials, 2013. **41**(0): p. 742-750.

29. Leemann, A., B. Münch, P. Gasser, and L. Holzer, *Influence of compaction on the interfacial transition zone and the permeability of concrete.* Cement and Concrete Research, 2006. **36**(8): p. 1425-1433.

30. Scrivener, K.L. and K.M. Nemati, *The percolation of pore space in the cement paste/aggregate interfacial zone of concrete.* Cement and Concrete Research, 1996. **26**(1): p. 35-40.

31. Zhang, C., A. Wang, M. Tang, and X. Liu, *The filling role of pozzolanic material.* Cement and Concrete Research, 1996. **26**(6): p. 943-947.

32. Jiang, J.-y., G.-w. Sun, and C.-h. Wang, *Numerical calculation on the porosity distribution and diffusion coefficient of interfacial transition zone in cement-based composite materials.* Construction and Building Materials, 2012.

33. Moon, H.Y., H.S. Kim, and D.S. Choi, *Relationship between average pore diameter and chloride diffusivity in various concretes.* Construction and Building Materials, 2006. **20**(9): p. 725-732.

Captured figures

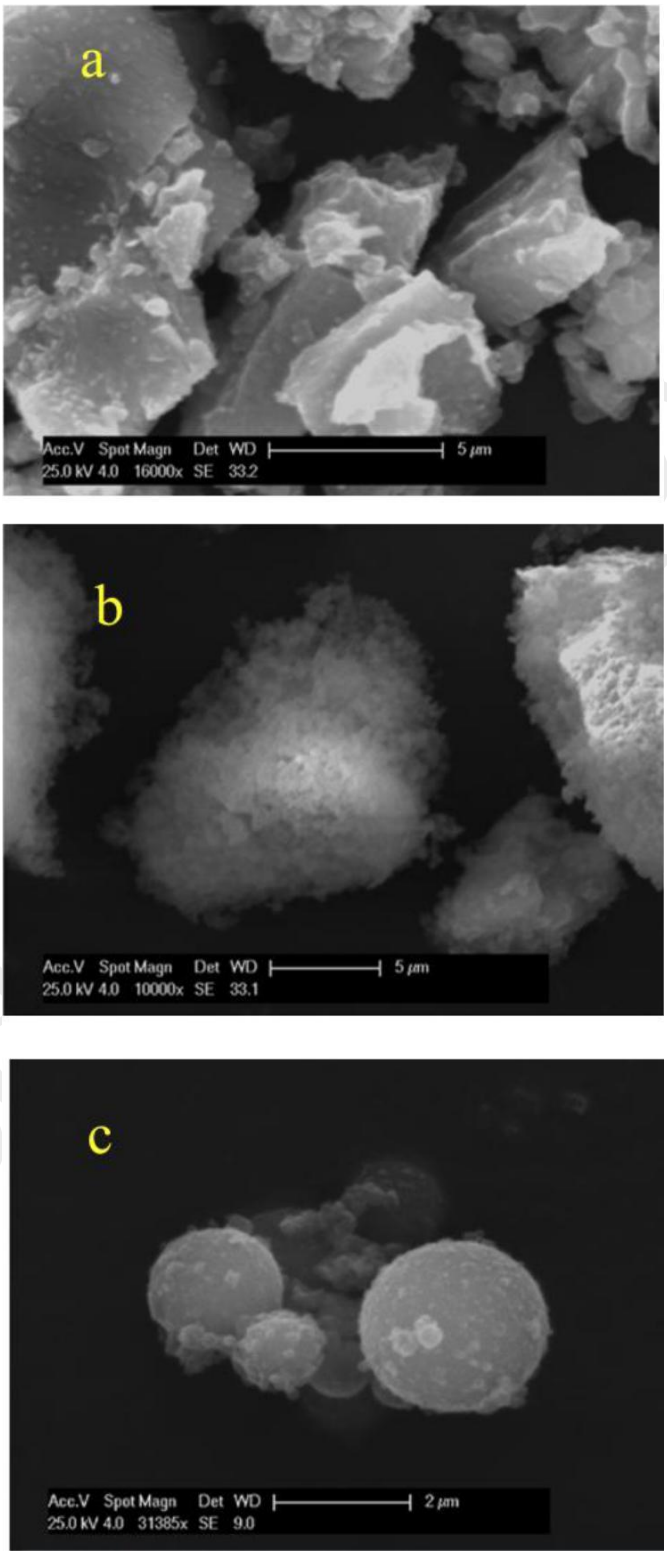

Figure 1 Selected SEM micrographs of: a) Cement b) Silica fume C) silica fume at high magnification

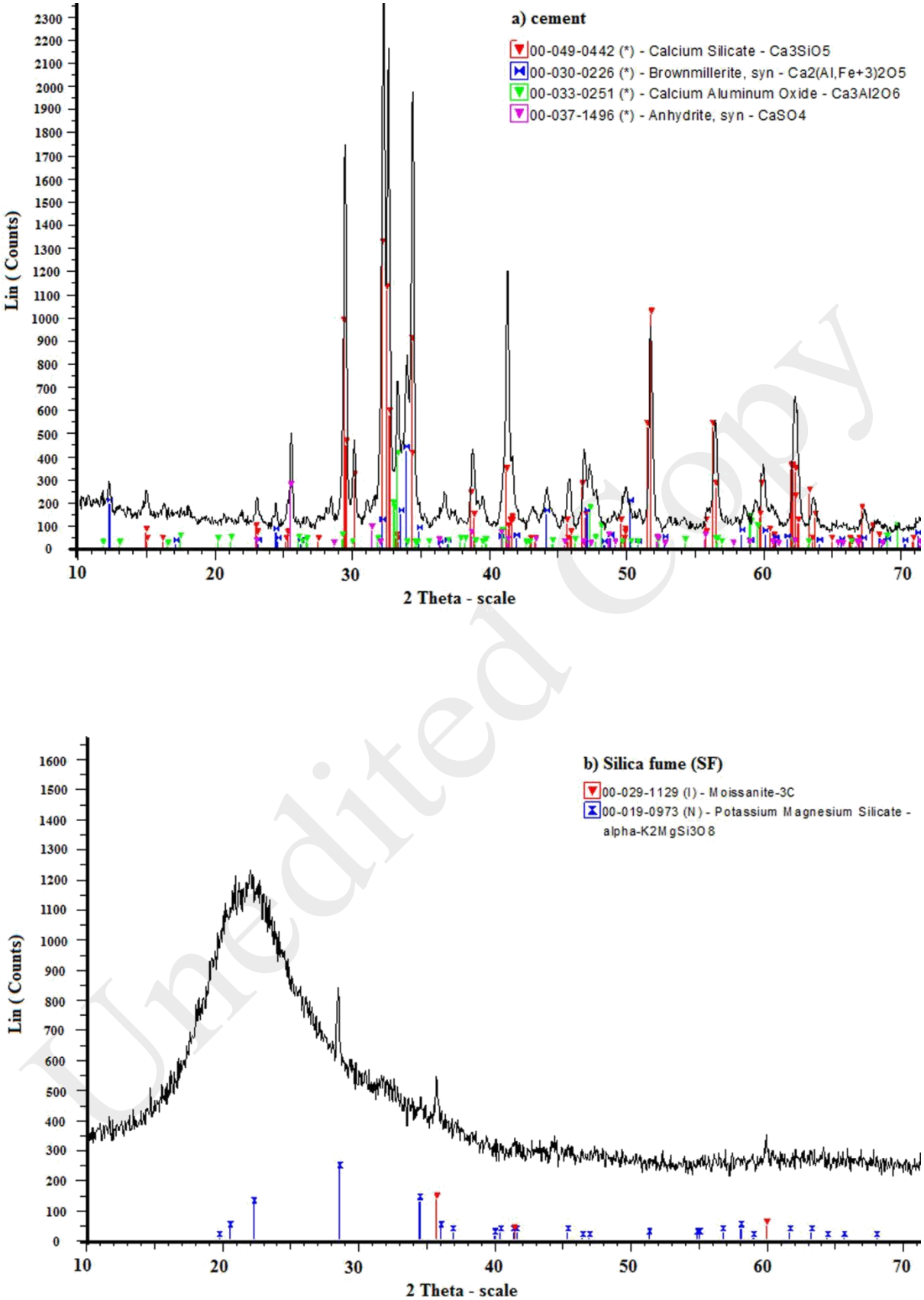

Figure 2 XRD spectra for: a) Cement b) Silica fume

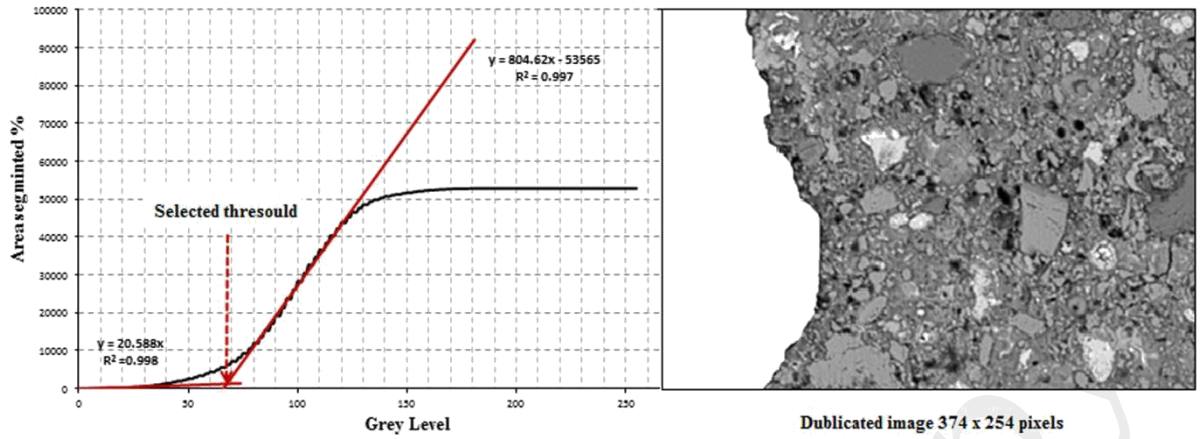

Figure 3 Example of the selection of upper porosity threshold using overflow method

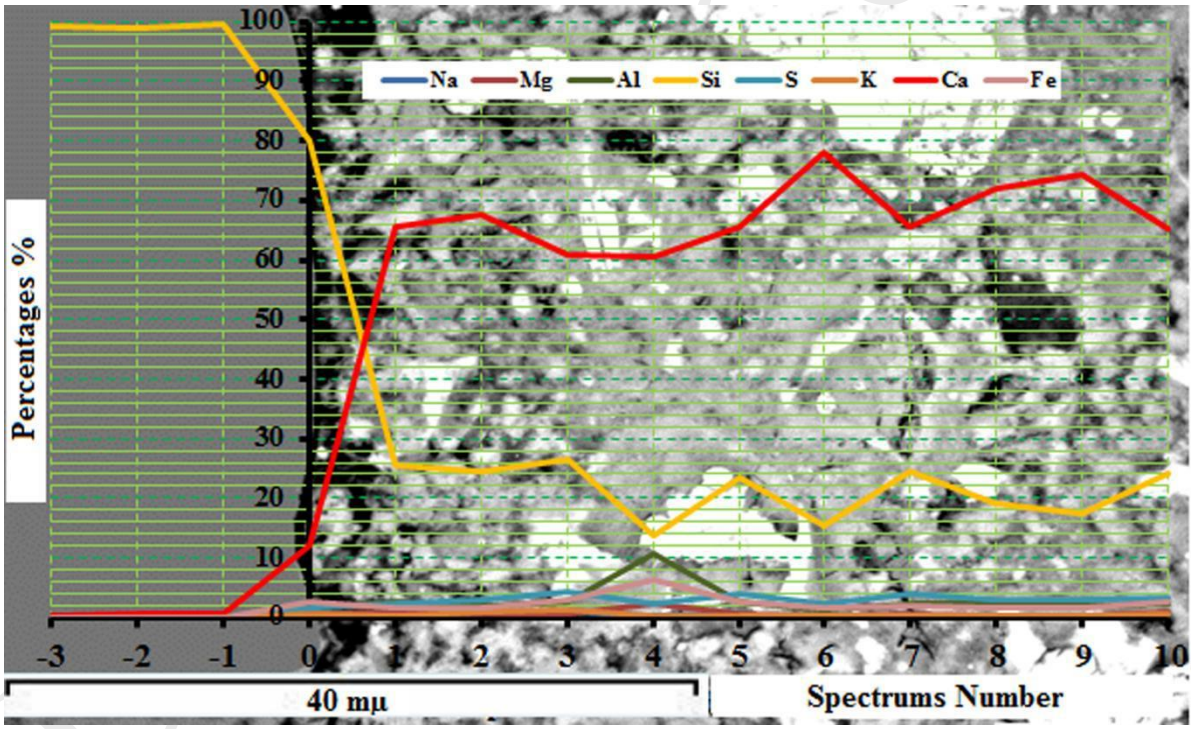

Figure 4 Example of X-ray line spectrum analyses (one line analysis for R-SCC)

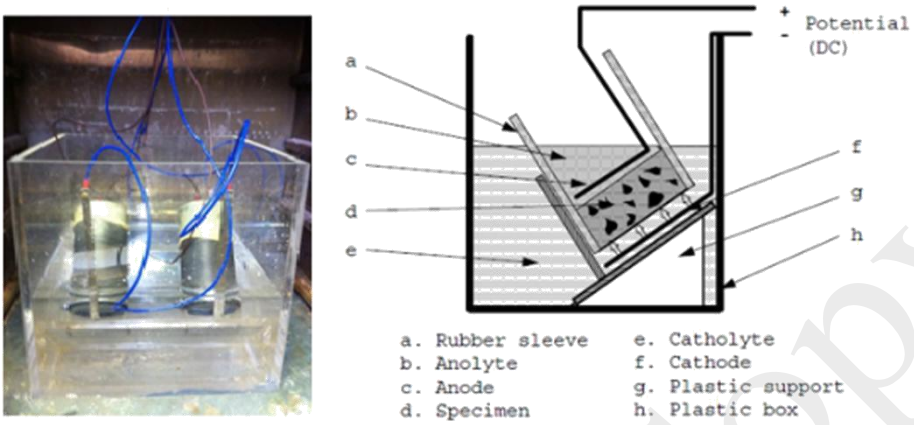

Figure 5 Photographs and schematic diagram for the rapid chloride migration test

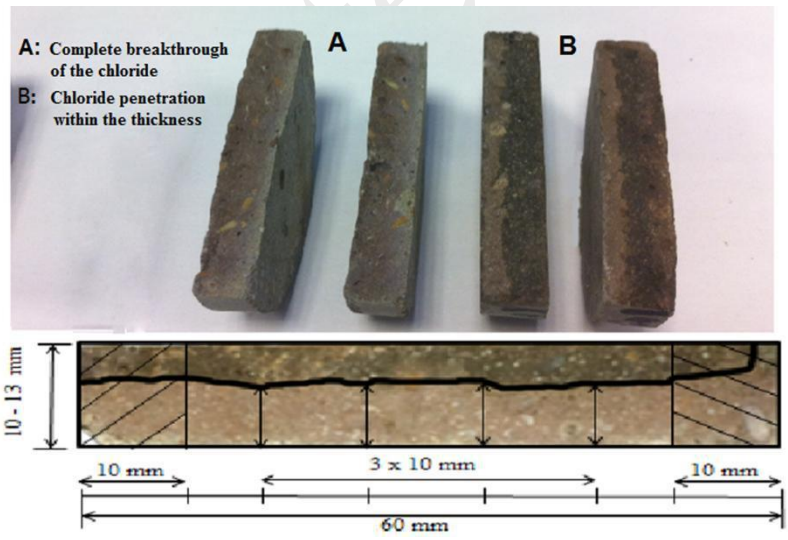

Figure 6 Examples of some tested specimens and the chloride penetration distance (x_d) revealed by AgCl

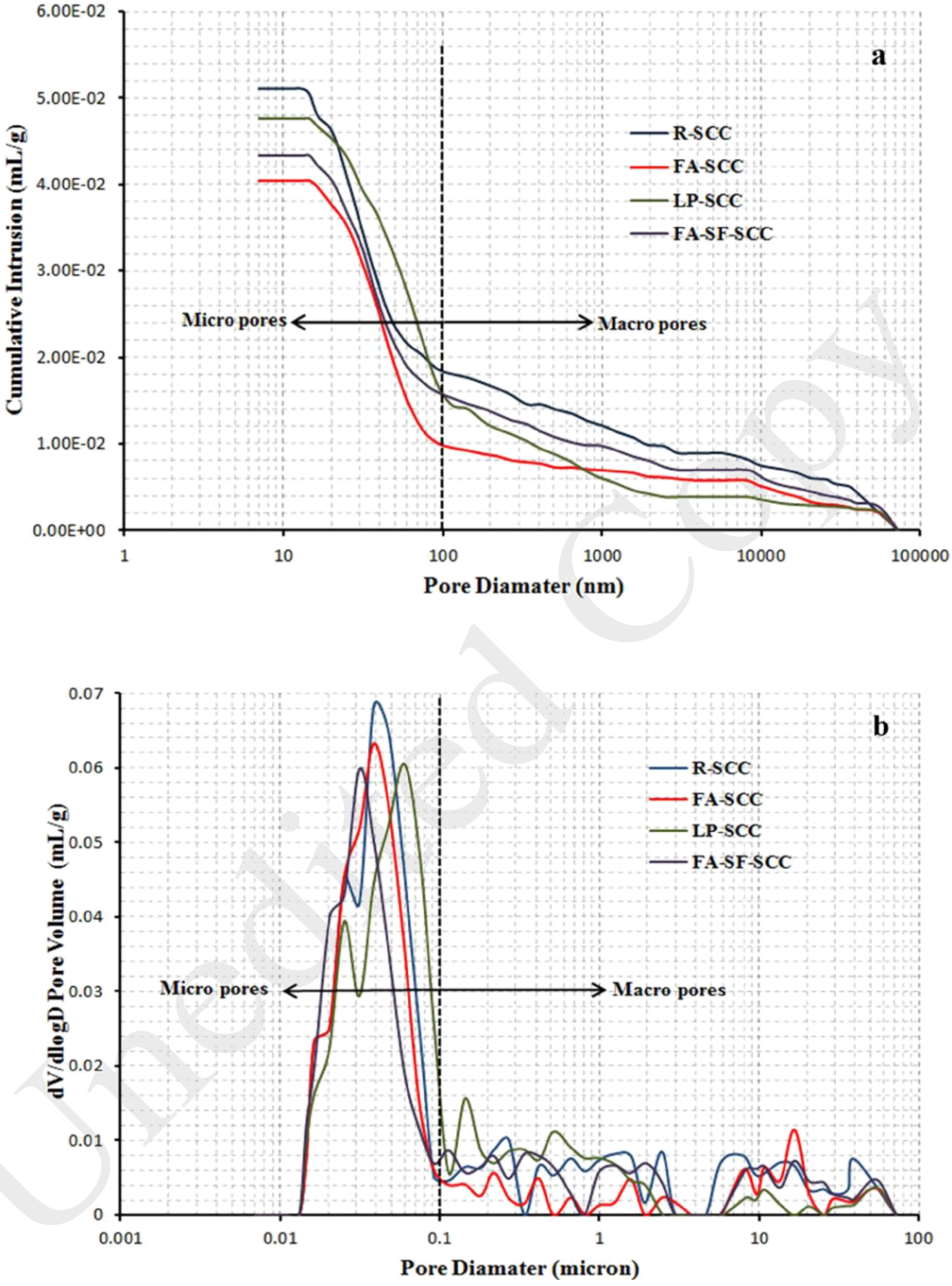

Figure 7 a) Mercury intrusion curves b) Derivatives of Mercury intrusion curves

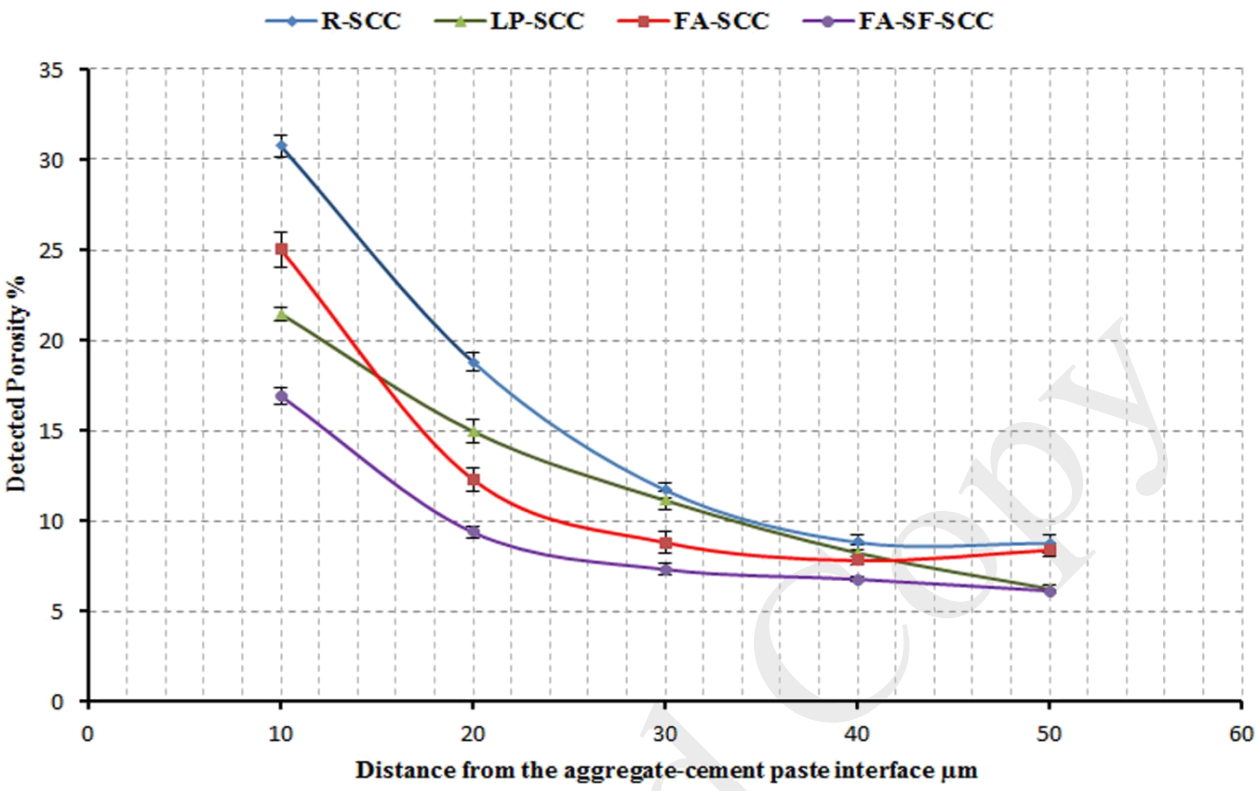

Figure 8 ITZ porosity profiles for the mixes

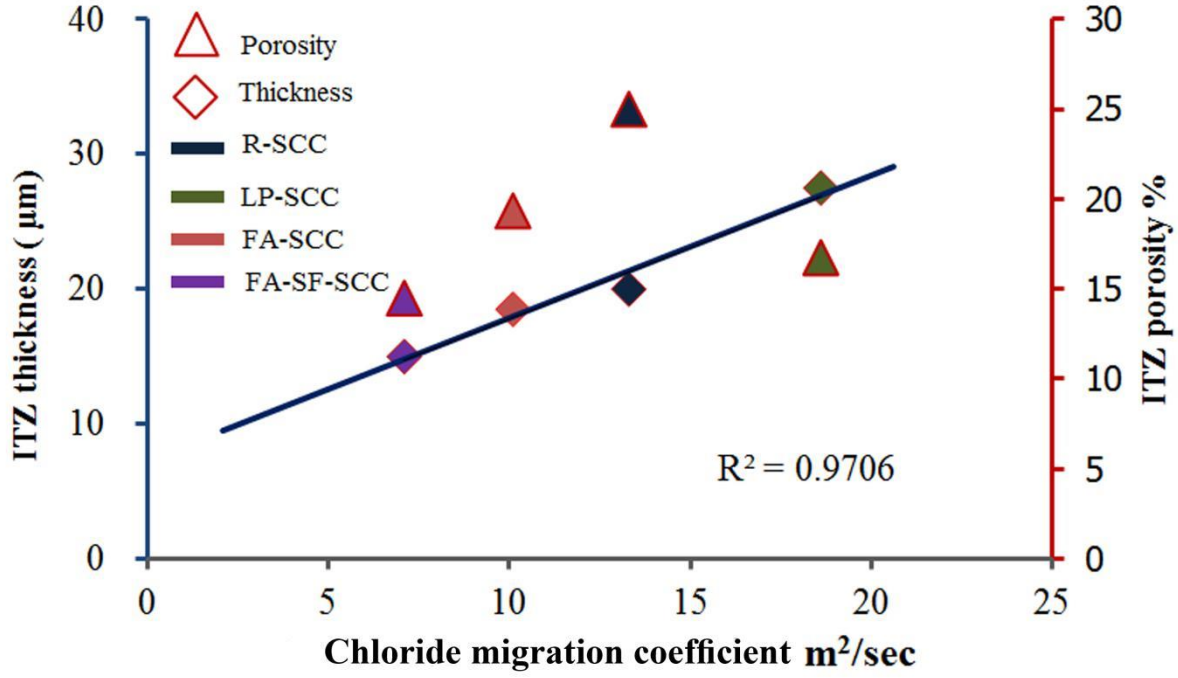

Figure 9 Relationship between the chloride migration coefficients, ITZs thicknesses and ITZs porosities

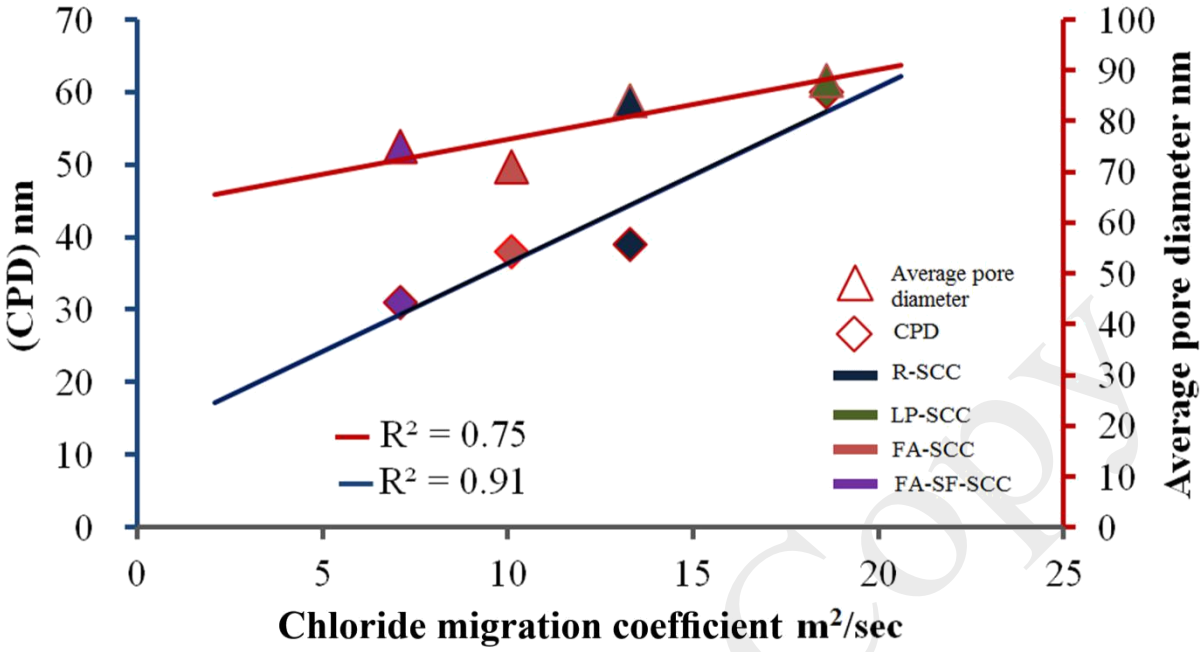

Figure 10 Relationship between the chloride migration coefficients and pore structure characteristics

Table 1 Chemical and physical properties of the used cement, fillers and mineral admixtures

Chemical compounds	Cement	Limestone (LP)	Fly ash (FA)	Silica fume (SF)
SiO_2	20.09	0.3	50%	> 90
Al_2O_3	4.84	---	26%	---
$CaCO_3$	---	99	---	---
Loss On Ignition	2.36	42.9	< 3	< 3
Specific gravity	3.15	2.7	2.21	2.2
Blain finesse m^2/kg	395	1550	388.5	22400

Table 2 Mix design and fresh requirements of SCC mixes

Mix type	R-SCC	LP-SCC	FA -SCC	FA-SF-SCC
Cement (kg/m^3)	450	300	300	300
Coarse agg. (kg/m^3)	875	860	825	825
Fine aggregate (kg/m^3)	900	900	900	900
Water (kg/m^3)	180	180	180	180
Fly ash (kg/m^3)	---	---	150	120
Limestone (kg/m^3)	---	150	---	---
Silica fume (kg/m^3)	---	---	---	30
$V_{coarse\ agg.}/V_{total}$	33.6	33.1	31.7	31.7
$V_{fine\ agg.}/V_{mortar}$	51.2	50.7	49.7	49.7
$V_{cement\ paste}/V_{total}$	32.3	33.0	34.3	34 .3
Slump flow (mm)	610	700	720	680
T50 (sec)	3.7	4.5	3.2	3.6
Bj (±2mm)	10	7.0	6.25	5
SI (%)	3	11.2	9.25	8.2
SP % by weight	3.9	2.6	1.83	3.1
Compressive Strength	56.1	50	56.5	57.9

T_{50}: time to obtain slump flow of 50 cm Bj: blocking step (J-ring test) SI: Segregation Index

Table 3 Internal pore characterizations at different scales (macro/micro and nano)

Mix ID	Micro pores % (MIP)	Macro pores % (MIP)	CPDs (nm) (MIP)	APDs (nm) (MIP)	Porosity% (MIP)	Porosity% (vacuum)	Micro pores % (Total)	Macro pores % (Total)
R-SCC	64.7	35.3	39	84	19.4	21.1	63	37
FA-SCC	75	25	38	71	8.7	14.7	69	31
LP-SCC	66.6	33.4	60	88	10.5	14.1	63	37
FA-SF-SCC	71	29	31	75	9.3	12.2	68.1	31.9

Table 4 Average Ca/Si ratio in the ITZ and cement matrix for SCC

Mix ID	R-SCC	LP-SCC	FA-SCC	FA-SF-SCC
Upper limit	3.68	19.1	4.6	3.1
Average Ca/Si ratio- ITZ	3.40	14.43	3.63	2.08
Lower limit	3.12	9.74	2.63	1.1
Upper limit	3.38	9.8	2.2	2.46
Average Ca/Si ratio- CM	3.16	8.285	1.99	2.17
Lower limit	2.93	6.77	1.7	1.88

Table 5 Overview of the pore structure, the ITZ features and the chloride migration coefficient results

Mix ID / Property	R-SCC	LP-SCC	FA-SCC	FA-SF-SCC	Evidence	Comment
Internal pore structure features						
Porosity % Macro/Micro	21.1 (Macro)	14.7 (Macro)	14.1 (Micro)	12.2 (Micro)	Vacuum saturated + MIP	Section 4.1
Pores features Nano scale (nm)	CPD/APD 39/84	CPD/APD 60/88	CPD/APD 38/71	CPD/APD 31/75	MIP	Section 4.1 and Fig.10
ITZ micro-permeation features						
ITZ porosity %	Rather high 25	Low 16.8	Low 19.4	Very low 14.5	Image analysis	Section 4.2 and Fig.10
ITZ thickness (μm)	Thin 19.9	Rather thick 27.5	Thin 18.5	Very thin 15	Image analysis	Section 4.2 and Fig.10
ITZ chemistry	Ca/Si=3.40 Intermixed (CH+CSH)	Ca/Si=14.43 Intermixed (CH+CSH)	Ca/Si=3.63 Intermixed (CH+CSH)	Ca/Si=2.08 high CSH content	EDX analysis	Section 4.3
ITZ percolation degree %	Very high 90%	High 88%	Very high 95%	High 78%	Winslow et al. [26]	Depends on ITZ thickness and the fine aggregate volume fraction
Chloride penetration velocity						
Chloride migration coefficient (Dnssm) m2/sec	13.3	18.6	10.1	7.1	Modified rapid migration test	Figs.9 and 10 correlates with pore structure and ITZ